Reduction of Cu_2O Islands Grown on a Cu(100) Surface through Vacuum Annealing

Guangwen Zhou* and Judith C. Yang

Department of Materials Science and Engineering, University of Pittsburgh, Pittsburgh, Pennsylvania 15261, USA

(Received 29 April 2004; published 22 November 2004)

The reduction of Cu_2O islands grown on Cu(100) surfaces through vacuum annealing was visualized by an *in situ* ultrahigh vacuum transmission electron microscope. The shrinkage of the island followed a linear decay behavior. The complete reduction of the oxide islands leads to the formation of nanoindentations on the Cu surfaces. A simple phenomenological kinetic model based on the dissociation along the island perimeter suitably describes the reduction behavior of the surface oxide islands.

DOI: 10.1103/PhysRevLett.93.226101 PACS numbers: 81.65.–b, 81.16.–c, 81.40.–z

The fundamental understanding of the reduction mechanism of oxides is important in many areas of physics, chemistry, and materials science and has an impact in practical applications including catalytic reactions, environmental stability, and electrochemistry. In particular, the stability of nanoscale structures has attracted intense interest with the rapid development of nanotechnology. Therefore, the understanding of the reaction mechanism at nanometer scale is essential. Two different phenomenological kinetic models, the "nucleation and growth model" and the "interface model," have been proposed for the reduction of oxides [1–4]. As shown schematically in Fig. 1(a), in the "nucleation and growth model," generation of small nuclei of the new phase (i.e., the reduced oxide) occurs on the oxide surface and the reaction interface increases until growing nuclei coalesce and then decreases, resulting in an induction period or a sigmoidal dependence of the extent of reaction, α, on time t. The early stage of the nucleation is usually described by a "power law" dependence of α on t and it changes to an "exponential law" after the coalescence of the nuclei [4]. In the "interface model," the rapid formation of a uniform and continuous layer of the reduced phase on the oxide surface occurs and the reaction boundary moves inward as the reaction proceeds, as shown in Fig. 1(b). The rate of oxide reduction is proportional to the area of the reduced-phase–oxide interface and the dependence of the reaction extent on t follows a similar "exponential law" as in the later stage of the "nucleation and growth model." Despite their difference in the initial reaction, a common assumption in these two models is that the reaction is of first order with respect to reactant [4], i.e., $-dC/dt = kC$, where dC/dt represents the rate change of reactant C with time t, and k is the rate constant. Many experimental systems involved in fundamental investigations of oxide reduction confirm the two models [5–10].

Recently it has been demonstrated that oxidation can be viewed as a processing tool for creating self-assembled oxide nanostructures on surfaces and these nanostructures exhibit peculiar properties [11–14]. The dynamic observation of the oxidation of Cu films by *in situ* transmission electron microscopy (TEM) reveals that completely different oxide nanostructures (disks, nanorods, container pyramids, cellular networks, etc.) can be obtained by altering the oxidation temperature and substrate orientation [15,16]. In this work we report the reduction of the epitaxial Cu_2O islands on Cu(100) surfaces visualized by *in situ* UHV-TEM, which provides both kinetic data by measuring the island shape and size in real time, and structural information by electron diffraction. Our observation demonstrates that the reduction of the epitaxial oxide islands follows a linear decay behavior and the island perimeter, which is defined as the contact line between the three phases of metal, oxide, and air, is the preferential reactive site for the oxide dissociation.

Our experiments were carried out in a modified JEOL 200CX TEM chamber [17]. A UHV chamber was attached to the middle of the column, where the base pressure is $<10^{-8}$ torr without the use of the cryoshroud. The microscope was operated at 100 keV to minimize irradiation effects. To avoid the possible electron beam induced oxide dissociation, the beam was on only when taking the images. Scientific grade oxygen gas of 99.999% purity can be admitted into the microscope column to oxidize the samples. Single crystal Cu(100) films were grown on irradiated NaCl(100) substrates in an

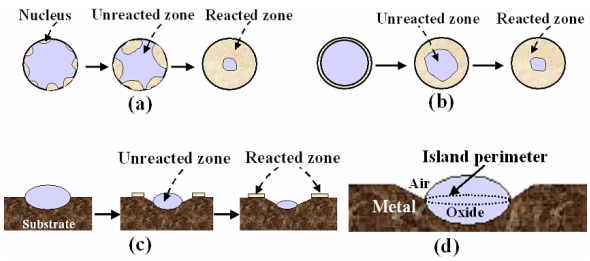

FIG. 1 (color online). Comparison of the previously proposed oxide reduction models—"nucleation and growth" model (a), "interface" model (b)—to our proposed "perimeter" model (c) in the reduction of surface oxide islands. The island perimeter is defined in (d).

UHV *e*-beam evaporation system. The Cu film was then removed from the substrate by dissolving the NaCl in deionized water and mounted on a specially prepared Si mount, where the modified microscope specimen holder allows for resistive heating of the specimen up to 1000 °C. The native Cu oxide was removed inside the TEM by annealing the Cu films in methanol vapor at a pressure of 5×10^{-5} torr and 350 °C, which reduces the copper oxides to copper [18]. The experiments include two steps, the first step is the creation of three dimensional Cu_2O islands on Cu(100) surface inside the microscope by *in situ* oxidation at oxygen pressure of 5×10^{-4} torr and temperatures ranging from 350 to 800 °C, Cu_2O islands grow into and out of the Cu film because of the ~59% volume increase during the oxidation of Cu to Cu_2O [15]. The amount of the embedding of the oxide into the Cu film depends on the oxidation temperature and oxidation time. After the oxide islands grow to the desired size, then the oxygen leaking is stopped and the microscope column can be pumped to 8×10^{-8} torr quickly by using the attached UHV pumps (turbo and ion pump). The reduction of the oxide islands can be visualized by *in situ* annealing of the oxidized Cu film inside the TEM chamber at the desired temperatures.

Reduction through the dissociation of the Cu_2O oxide is described by $Cu_2O(s) \rightarrow 2Cu^0(s) + O(g)$. Therefore, the reduction of Cu_2O to Cu^0 is accompanied by the formation of new Cu and molecular oxygen desorbed from the surface due to the small solubility of oxygen in bulk copper [19,20]. Figure 2(a) is a bright-field (BF) TEM micrograph showing the morphology of the Cu film, where the oxide islands have an initial reduction at 800 °C for ~2 min. The dark contrast around the islands is due to the formation of the reduced-phase (Cu) layer on the substrate surface, as confirmed by electron diffraction. The reduction of the oxide islands results in the reduced phase on the substrate surface around the islands, rather than filling up the space left by the oxide. The formation of the reduced phase verifies that reduction, instead of vaporization, occurred during thermal annealing. The fourfold symmetry of the newly formed Cu layer is related to the (100) surface structure of the Cu substrate. The contrast feature along the island perimeter [Fig. 2(a)] indicates that the island perimeter is the preferred site for the dissociation of the oxide. This is confirmed by the atomic force microscopy (AFM) image of the partially reduced oxide islands as shown in Fig. 2(b), where the surface profile analysis reveals a trench along the island perimeter and the height of the newly formed Cu layer is ~10 nm.

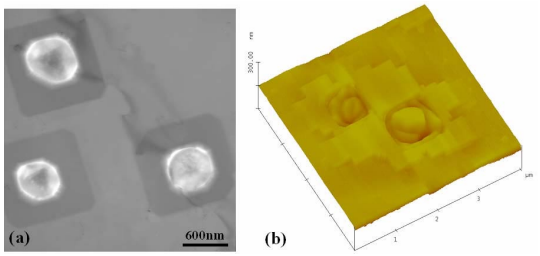

FIG. 2 (color online). (a) The initial stages of the island reduction; (b) AFM image of partially reduced oxide islands.

The detailed size evolution of the oxide islands under the isothermal annealing can be followed inside the microscope. Figure 3(a) is a sequential time series of the reduction of two oxide islands at 750 °C. The islands have a circular shape on the substrate surface, and the reduction of the islands results in the formation of a new Cu layer on the substrate, causing the dark contrast around the islands. Figure 3(b) is a plot of the island areas versus reduction time, and a linear decay behavior is noticed. In the following, we present a model based on the dissociation along the island perimeter to explain the observed linear decay behavior of the oxide islands.

The reduction process of the island is described as follows. The dissociation of Cu_2O along the island perimeter results in Cu atoms and oxygen, where the Cu atoms diffuse to the substrate surface around the island which provides a perfect template for the formation of the new Cu layer, and the oxygen is desorbed from the surface as molecular oxygen due to its small solubility in bulk Cu [19,20]. Therefore, the Cu atoms in the oxide lattice are displaced to the substrate surface and this causes the formation of the indentation on the substrate surface. Figures 1(c) and 1(d) are a schematic diagram of the "perimeter model" for the reduction of surface oxide islands. The dissociation along the island perimeter creates a shrinkage rate

$$\frac{dN(t)}{dt} = -CLJ, \tag{1}$$

where $N(t)$ is the total number of Cu atoms in a Cu_2O island at time t, C is the dissociation coefficient, J is the diffusive flux of copper atoms leaving the islands, and L is the island perimeter. Since the lateral size of the island on the substrate surface is much larger than its thickness, we assume that the island has an ellipsoid shape, and

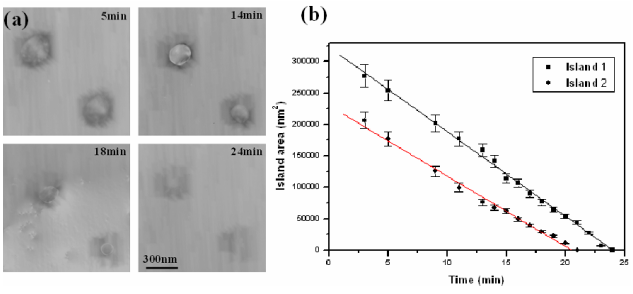

FIG. 3 (color online). (a) The *in situ* observation of the reduction of two oxide islands at 750 °C; (b) the dependence of the area of the two islands on the reduction time, the solid lines correspond to the theoretical fit to the "perimeter model."

solve Eq. (1), it is found that the island cross-sectional area decreases linearly with respect to the reduction time

$$A = A_0 - \frac{\Omega \pi J C}{\beta} t, \tag{2}$$

where Ω is the atomic volume of Cu in Cu_2O, β is the aspect ratio of the oxide island, A_0 is the cross-section area of the island before reduction. The solid lines in Fig. 3(b) represent the theoretical fit of the experimental data by Eq. (2), and the slope corresponds to the rate constant. Since the two islands have similar shapes and the same reduction conditions, then their reduction rate constants should be similar as is confirmed in Fig. 3(b). Equation (2) indicates that the rate constant, $K = \Omega \pi J C/\beta$, is related to island geometry, diffusion of Cu atoms, and the dissociation coefficient at the island perimeter. For the reduction reaction at these high temperatures ($> 750\,^{\circ}C$), the mass transport processes such as the surface diffusion of Cu atoms on the Cu substrate and the migration of point defects in the oxide islands are very fast. The dissociation of Cu_2O along the island perimeter is considered to be the rate-determining step in the reaction. This can be understood by considering the specific energy required in these different steps. The dissociation energy of Cu_2O is $\sim$1.7 eV estimated from its formation enthalpy. Cu_2O is known as a cation-deficient semiconductor and the activation energy for the point defect migration in Cu_2O is known as $\sim$1 eV [21,22]. The activation energy for surface diffusion of Cu atoms on Cu is $\sim$0.5 eV [23,24]. Therefore, higher activation energy is needed for the oxide dissociation than the other steps in the reduction reaction. This energetics barrier responsible for the detachment-limited kinetics was reported in the decay of Cu islands on Cu surface, and the linear shrinkage of the island area was also observed [25,26].

We also investigated the lattice structure near the Cu and Cu_2O interface by high resolution transmission electron microscopy (HRTEM). The HRTEM images reveal that the Cu lattice appears undistorted with no defects or strain, but a lot of lattice distortions occur in the oxide island. These lattice distortions are caused by the growth stress because of the 59% volume increase accompanied with the oxide formation. The Young's modulus (E) and shear modulus (G) of copper is $\sim$124 and $\sim$40 GPa, respectively, which is much larger than that of Cu_2O ($E =$ 30 GPa, $G = 10$ GPa), even considering their temperature dependence [27]. The metallic Cu around the islands catalyzes the reduction of the oxide by facilitating the nucleation of the additional Cu from the reducing Cu_2O islands. The dissociation of the oxide along the island perimeter provides the easiest pathway for the reaction, not only for the transport and crystallization of the reduced phase, but also for the release of the interface strain and volume strain in the oxide.

The other mechanisms such as the Cu_2O dissociation on the oxide surface or the surface plus the island perimeter are unlikely based on the present investigation. The theoretical analysis of the oxide reduction by the dissociation on the island surface gives a power law dependence of the island area on the reduction time, and a more complex dependence for the dissociation along the island perimeter and surface area [16]. Also, the formation of the deep trench between the metal and oxide is not expected for the reduction controlled by the dissociation on the oxide surface or inside the oxide. The present investigation is focused on the thermal reduction of the oxide islands at high temperatures in vacuum. In many technological applications the oxide is reduced to lower temperatures by reaction with H_2 and/or CO. One could think that in this cases, the reduction mechanism would be different from that presented here, because the reactants (H_2 or CO) could adsorb on the oxide surface and penetrate into the oxide lattice [6].

The reduction of the surface oxide by this perimeter mechanism provides a simple way to create nanoindentation arrays on surfaces. Figure 4(a) is a BF TEM micrograph of the Cu film after the complete reduction of the oxide islands, where the Cu film was first oxidized at $800\,^{\circ}C$ and oxygen pressure of $\sim 5 \times 10^{-4}$ torr for $\sim$10 min to create the Cu_2O island array on the Cu surface. The areas with the bright contrast in the micrograph are the thinned regions due to the reduction of the oxide. The inset in Fig. 4(a) shows an intermediate shape of a Cu_2O island before the complete reduction. The original island had a square shape and the crystallographic relationship between the island and the Cu film is cube on cube and the normal to the edges of the island is $(110)Cu_2O//(110)Cu$. Figure 4(b) is an AFM image from the same Cu film, which reveals the nanoindentation array formed on the surface.

In conclusion, the reduction of the epitaxail Cu_2O islands on Cu(100) surface created by nanooxidation

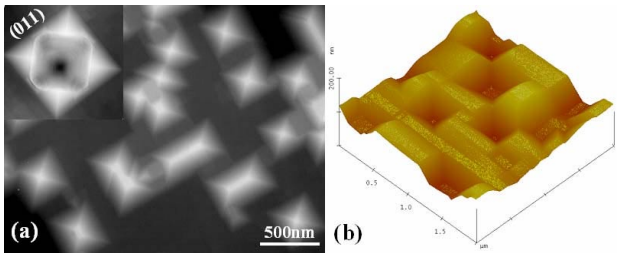

FIG. 4 (color online). (a) Bright-field TEM image of the Cu(100) film after the complete reduction of the oxide islands, the area with bright contrast is the thinned regions due to the oxide reduction, the inset is an intermediate shape of an island during the reduction; (b) an AFM image showing the surface topology of the Cu film after the oxide reduction, which reveals the nanoindentation array formed on the surface, where the typical depth of the indentation is $\sim$15 nm.

was investigated by an *in situ* UHV-TEM. The kinetic data on the size evolution of the islands during the reduction reaction agree well with a perimeter dissociation model. These types of *in situ investigations* provides unique understanding in phase transitions and phase stabilities of surface oxide nanostructures. The complete reduction of the oxide islands by this dissociation mechanism leads to the formation of nanoindentation arrays on metal surfaces. Island formation during oxidation has been observed in several other metal systems, such as Ni, Fe, Ti, Co, Pd, Ir, Sn, as well as in Cu. By carefully choosing the oxidation-reduction conditions, such as temperature, oxygen pressure, substrate orientation, etc., we expect our results are more general and the nanoindentation arrays could be realized in these metal systems which can serve as building blocks for the development of nanodevices.

This research project is funded by the National Science Foundation (DMR No. 9902863), the Department of Energy (DEFG02-96ER45439), and National Association of Corrosion Engineers seed grant. We are thankful to the Materials Research Laboratory, University of Illinois at Urbana-Champaign for experimental facilities. The authors kindly thank I. Petrov, R. Twesten, M. Marshall, K. Colravy, and N. Finnegan for their help.

*Present address: Materials Science Division, Argonne National Laboratory, Argonne, IL 60439, USA.

[1] B. Delmon, *Handbook of Heterogeneous Catalysis*, edited by G. Ertl, H. Knozinger, and J. Weitkamp (Wiley-VCH, New York, 1997).
[2] H. H. Kung, *Transition Metal Oxides: Surface Chemistry and Catalysis* (Elsevier, New York, 1989).
[3] J. J. Scholz and M. A. Langell, Surf. Sci. **164**, 543 (1985).
[4] *Comprehensive Chemical Kinetics*, edited by C. H. Bamford, C. F. H. Tipper, and R. G. Compton (Elsevier, New York, 1984), Vol. 21.
[5] J. A. Rodringuez, J. C. Hanson, A. I. Frenkel, J. Y. Kim, and M. Perez, J. Am. Chem. Soc. **124**, 346 (2002).
[6] J. Y. Kim, J. A. Rodriguez, J. C. Hanson, A. I. Frenkel, and P. L. Lee, J. Am. Chem. Soc. **125**, 10684 (2003).
[7] J. G. Chen, D. A. Fischer, J. H. Hardenbergh, and R. B. Hall, Surf. Sci. **279**, 13 (1992).
[8] R. P. Furstenau, G. Mcdougall, and M. A. Langell, Surf. Sci. **150**, 55 (1985).
[9] T. Ressler, R. E. Jentoft, J. Wienold, M. M. Gunter, and O. Timpe, J. Phys. Chem. B **104**, 6360 (2000).
[10] J. A. Rodringuez, J. Y. Kim, J. C. Hanson, M. Perez, and A. I. Frenkel, Catal. Lett. **85**, 247 (2003).
[11] S. Aggarwal, A. P. Monga, S. R. Perusse, R. Ramesh, V. Ballarotto, E. D. Williams, B. R. Chalamala, Y. Wei, and R. H. Reuss, Science **287**, 2235 (2000).
[12] S. Aggarwal, S. B. Ogale, C. S. Ganpule, S. R. Shinde, V. A. Novikov, A. P. Monga, M. R. Burr, R. Ramesh, V. Ballarotto, and E. D. Williams, Appl. Phys. Lett. **78**, 1442 (2001).
[13] S. R. Shinde, A. S. Ogale, S. B. Ogale, S. Aggarwal, V. A. Novikov, E. D. Williams, and R. Ramesh, Phys. Rev. B **64**, 035408 (2001).
[14] A. S. Ogale, Phys. Rev. B **64**, 035409 (2001).
[15] G. W. Zhou and J. C. Yang, Phys. Rev. Lett. **89**, 106101 (2002); Appl. Surf. Sci. **210**, 165 (2003); Surf. Sci. **531**, 359 (2003); Appl. Surf. Sci. **222**, 357 (2004); Surf. Sci. **559**, 100 (2004).
[16] G. W. Zhou, Ph.D. thesis, University of Pittsburgh, 2003.
[17] M. L. McDonald, J. M. Gibson, and F. C. Unterwald, Rev. Sci. Instrum. **60**, 700 (1989).
[18] S. M. Francis, F. M. Leibsle, S. Haq, N. Xiang, and M. Bowker, Surf. Sci. **315**, 284 (1994).
[19] M. Hansen, *Constitution of Binary Alloys* (McGraw-Hill, New York, 1958).
[20] R. L. Pastorek and R. A. Rapp, Trans. Metall. Soc. AIME **245**, 1711 (1969).
[21] A. F. Wright and J. S. Nelson, J. Appl. Phys. **92**, 5849 (2002).
[22] N. L. Peterson and C. L. Wiley, J. Phys. Chem. Solids **45**, 281 (1984).
[23] G. Boisvert, N. Mousseau, and L. J. Lewis, Phys. Rev. B **58**, 12 667 (1998).
[24] Z. Y. Wang, Y. H. Li, and J. B. Adams, Surf. Sci. **450**, 51 (2000).
[25] W. L. Ling, N. C. Bartelt, K. Pohl, J. de la Figuera, R. Q. Hwang, and K. F. McCarty, Phys. Rev. Lett. **93**, 166101 (2004).
[26] J. B. Hannon, C. Klunker, M. Giesen, and H. Ibach, Phys. Rev. Lett. **79**, 2506 (1997).
[27] H. J. Frost and M. F. Ashby, *Deformation-Mechanism Maps* (Pergamon, Oxford, 1982).